AD-A174 990 MATERIAL STRUCTURE IN VISCOPLASTICITY: AN EXTENSION OF BODNER'S THEORY(U) BATTELLE PACIFIC NORTHWEST LAB RICHLAND WA R E WILLIFORD 15 JUL 86 AFOSR-TR-86-2125 1/1

UNCLASSIFIED F49620-85-C-0149 F/G 20/11 NL

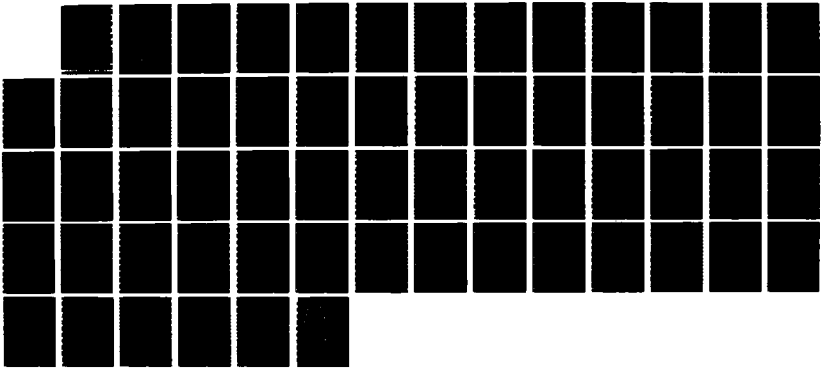

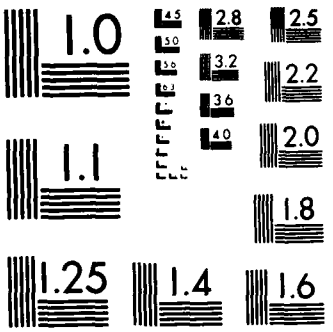

AFOSR-TR- 86-2125

Material Structure in Viscoplasticity: An Extension of Bodner's Theory

Final Report

R. E. Williford

July 1986

Prepared for
U. S. Air Force
Office of Scientific Research
under Contract F49620-85-C-0149

Battelle
Pacific Northwest Laboratories

FINAL REPORT

MATERIAL STRUCTURE IN VISCOPLASTICITY: AN EXTENSION OF BODNER'S THEORY

R. E. Williford

July 1986

Prepared for
U.S. Air Force
Office of Scientific Research
under Contract F49620-85-C-0149

Battelle
Pacific Northwest Laboratories
Richland, Washington 99352

SECURITY CLASSIFICATION OF THIS PAGE

REPORT DOCUMENTATION PAGE

1a. REPORT SECURITY CLASSIFICATION None	1b. RESTRICTIVE MARKINGS None
2a. SECURITY CLASSIFICATION AUTHORITY	3. DISTRIBUTION / AVAILABILITY OF REPORT Approved for public release; distribution unlimited. Unrestricted
2b. DECLASSIFICATION / DOWNGRADING SCHEDULE	
4. PERFORMING ORGANIZATION REPORT NUMBER(S) 2311106833	5. MONITORING ORGANIZATION REPORT NUMBER(S) AFOSR-TR- 86-2125
6a. NAME OF PERFORMING ORGANIZATION Battelle-Northwest Battelle Memorial Institute 6b. OFFICE SYMBOL (If applicable)	7a. NAME OF MONITORING ORGANIZATION AFOSR - Directorate of Aerospace Sciences
6c. ADDRESS (City, State, and ZIP Code) P.O. Box 999 Richland, WA 99352	7b. ADDRESS (City, State, and ZIP Code) Building 410 Bolling AFB Washington, DC 20332-6448
8a. NAME OF FUNDING / SPONSORING ORGANIZATION AFOSR 8b. OFFICE SYMBOL (If applicable) NA	9. PROCUREMENT INSTRUMENT IDENTIFICATION NUMBER ~~AFOSR Contract~~: F49620-85-C-0149
8c. ADDRESS (City, State, and ZIP Code) Bolling AFB Washington, DC 20332-6448	10. SOURCE OF FUNDING NUMBERS PROGRAM ELEMENT NO. 61102 / PROJECT NO. 2302 / TASK NO. B1 / WORK UNIT ACCESSION NO.

11. TITLE (Include Security Classification)

Material Structure in Viscoplasticity: An Extension of Bodner's Theory

12. PERSONAL AUTHOR(S)
Williford, R. E.

13a. TYPE OF REPORT	13b. TIME COVERED	14. DATE OF REPORT (Year, Month, Day)	15. PAGE COUNT
Final	FROM 9/1/85 TO 5/31/86	7/15/86	59

16. SUPPLEMENTARY NOTATION

17. COSATI CODES			18. SUBJECT TERMS (Continue on reverse if necessary and identify by block number)
FIELD	GROUP	SUB-GROUP	Viscoplasticity, Bodner's Theory; microstructure; fractals; scalings; nonlocal stress polarization.

19. ABSTRACT (Continue on reverse if necessary and identify by block number)

Although Bodner's viscoplastic constitutive equation is useful because it does not require a yield criterion, it also exhibits deficiencies related to hardening behavior. Two new constitutive forms were developed from Bodner's equation to address this problem. The general approach employed scaling relations to define macrostructural response in terms of microstructural evolution. The first new equation expresses strain rate as a function of scaled microstructural models available from the metallurgical literature, and is useful for structural analyses. The second new equation represents a nonlocal model for viscoplasticity. It describes the evolution of internal stress field fluctuations in terms of scaled hardening and damage state variables, and contains the basis for a new material state tensor. The two new equations were verified by comparison to creep data for a steel alloy and aluminum, respectively.

20. DISTRIBUTION / AVAILABILITY OF ABSTRACT	21. ABSTRACT SECURITY CLASSIFICATION
☒ UNCLASSIFIED/UNLIMITED ☐ SAME AS RPT. ☐ DTIC USERS	
22a. NAME OF RESPONSIBLE INDIVIDUAL R.E. Williford Dr. Salkind	22b. TELEPHONE (Include Area Code) ~~(509) 375-2956~~ 767-4987
22c. OFFICE SYMBOL NA	

DD FORM 1473, 84 MAR 83 APR edition may be used until exhausted. All other editions are obsolete.

SECURITY CLASSIFICATION OF THIS PAGE

CONTENTS

A-1

FIGURES

1.0 SUMMARY

Bodner's constitutive equation [1-5] is one of those used by the U.S. Air Force to model viscoplastic deformation. This particular equation is useful because of its relative mathematical simplicity, partly due to the elimination of the need for a yield surface. However, Bodner's formulation is not without problems, such as difficulties in fitting the material constants of the equation to data [6], and a general deficiency of the model to properly account for hardening phenomena [7]. Deficiencies in the hardening behavior of Bodner's equation likewise imply that similar deficiencies probably exist for the softening behavior caused by the accumulation of material damage in the form of voids or microcracks. These deficiencies led to the definition of the present work, the objectives of which were:

(1) to improve the capabilities of Bodner's viscoplastic constitutive equation for modeling deformation-induced hardening phenomena by incorporating microstructural models into the equation, and

(2) to develop a continuum formulation that simultaneously represents the mechanics of both hardening and damage behavior, with the ultimate aim of developing a new material state tensor.

The first objective has been accomplished. The second objective is about 50% accomplished at this writing, and work required for completion has been defined. These results are briefly described in the following paragraphs.

Bodner's constitutive equation in uniaxial form is:

$$\dot{\varepsilon} = \dot{\varepsilon}_0 \exp\left[-C\left(\frac{Z}{\sigma}\right)^n\right] \tag{1.1}$$

where $\dot{\varepsilon}$ is the strain rate, $\dot{\varepsilon}_0$ is the maximum strain rate, C and n are material constants, Z is the hardening parameter, and σ is the stress. The first objective was to express this equation in a form that would readily admit

microstructural models from the metallurgical literature. This was accomplished using some recent developments in mathematics which are particularly suited for the development of scaling relations. The "new mathematics" are called fractals, and are geometric forms which are very useful for concisely representing the complexity of nature. The reader is referred to [8] and Section 2.2 of this report for descriptions and examples, with the notation that only the simplest scaling concepts of fractals were used to obtain the following result:

$$\dot{\varepsilon}_s = \dot{\varepsilon}_o \exp\left[\frac{\text{Physics Data}}{\text{Engrg. Data}} (M_1 M_2 M_3 \ldots)\right] \tag{1.2}$$

where $\dot{\varepsilon}_s$ is the macroscopic strain rate. "Physics Data" are known quantities on the atomic scale, such as atomic binding energy. "Engineering Data" are measured quantities on the macroscopic scale, such as stress. M_1, M_2... represent microstructural phenomena on intermediate scales, described by models available from the metallurgical literature. Examples are M_1 = the number of atoms per unit length dislocation, M_2 = the number of dislocations per dislocation cell. In general, any number of M's may be employed for arbitrarily selected intermediate scales as long as the first scale relates to the atomic behavior, and the last scale relates to the macroscopic sample behavior. The formulation is quite general. Its flexibility permits versatile use in structural analysis computer codes because various M's may be inserted in or deleted from Equation (1.2) at will as performance variables (i.e., temperature) change during a simulation. The above results are described in Section 3 of this report.

The second objective was to develop a continuum representation that unites deformation (hardening) and damage (softening) mechanics, with the ultimate aim of developing a new material state tensor. This effort began with an analysis of a fractal form of the conservation of mass equation, but the first attempt was abandoned when it was found that hardening and damage phenomena remained separated and could not be uniquely combined in this approach. These results are described in more detail in the Appendix.

The second attempt to accomplish objective (2) was successful. This approach combined fractal scalings with concepts from the "nonlocal" theories of continuum mechanics. Nonlocal theories characterize the effects of material inhomogeneities (i.e., hardening and damage substructures) on macroscopic performance by including a fundamental measure of length in the formulations. This length parameter characterizes the spacing between the microstructural features which control the material response, or the ranges of the fluctuations in the stress and strain fields within the material. Internal stress field fluctuations are sometimes called "stress polarization." Insertion of fractal scaling relations into Bodner's Equation resulted in the development of a rather complicated expression for the stress polarization (fluctuations), σ_p, on any scale m within the deforming material:

$$\sigma_{pm} = f[g(r_m),\ dE_m/dr_m,\ \dot{\varepsilon}_s,\ \sigma_s] \tag{1.3}$$

where $g(r_m)$ is a deformation-dependent scale function, E_m is the effective modulus at scale m<s, the subscript s denotes the macroscopic sample scale, and r_m is a function of the volume fractions of hardening and damage substructures (ϕ_{hm}, ϕ_{dm}) at scale m. The modulus term in Equation (1.3) is given by a particular effective medium theory [9,10]. Both $g(r_m)$ and the modulus term depend on ϕ_{hm}, ϕ_{dm}, and b_m, where the latter is a numerical scale factor (length parameter) chosen at will. Note that ϕ_{hm}, ϕ_{dm}, and b_m are all measurable, so that experimental verification is possible. The function r_m provides the basis for defining the new hardening/damage state tensor in terms of measures of departure from an identity tensor, which in turn can be introduced into standard continuum formulations. Equation (1.3) thus provides the foundation for accomplishing the second major objective stated above.

Because of the mathematical complexity of Equation (1.3), this goal could not be fully attained within the resources of this project. However, preliminary results concerning the numerical verification of Equation (1.3) are shown in Section 4.2. It should be noted that accomplishment of the second objective will also provide an engineering tool which apparently does not presently exist: a nonlocal theory for rate-dependent deformation, where substructural

"inhomogeneities" evolve rather than having been completely specified from the initial geometry of the problem, as in a composite. Engineering applications of such a development include prediction of the deformation-dependent spectrum of scales over which nonlocal behavior dominates. This in turn provides guidance concerning the proper magnifications needed for metallographic examinations to fully reveal the substructural features that control deformation behavior.

The balance of this report begins with the Background, which includes brief descriptions of Bodner's Theory and fractals. This is followed by a summary of the work performed to accomplish the first objective above: the incorporation of microstructural models into Bodner's Equation. Section 4 describes work performed toward accomplishing the second objective, and contains the complete development of the so-named stress polarization equation. Conclusions and Recommendations are summarized in the final section.

2.0 BACKGROUND

2.1 BODNER'S EQUATION AND THE STATE VARIABLE APPROACH

A number of mathematical approaches are available for the constitutive modeling of rate-dependent deformation processes [11], each having unique advantages and disadvantages concerning physical meaning, developmental costs, and degree of success in application. One of the most effective approaches is the state variable method, which combines macroscopic stress-strain rate relations with judiciously selected microstructural observations. This is accomplished by the specification of both a kinetic "equation of state" which contains microstructural "state parameters", and supplementary equations describing the evolution of those parameters with deformation. An example of such a kinetic equation is the uniaxial form of Bodner's Law shown in Equation (1.1), which describes the relation between plastic strain rate ($\dot{\varepsilon}$) and stress (σ). The foundations for this equation are summarized in the following two paragraphs.

Briefly, Bodner decomposes the deformation rate tensor into elastic and plastic components [1-5]

$$d_{ij} = d^e_{ij} + d^p_{ij} \tag{2.1}$$

where d_{ij} is the symmetric part of the material velocity gradient

$$d_{ij} = 1/2\ (V_{i,j} + V_{j,i}) \tag{2.2}$$

The flow rule employed is a generalized Prandtl-Reuss law

$$d^p_{ij} = F(J_2,Z,T)\ S_{ij} \tag{2.3}$$

where S_{ij} is the deviatoric stress tensor, J_2 is the second invariant of S_{ij}, T is temperature, and Z is an internal state parameter. Squaring Equation (2.3), we have

$$F^2 = D_2^p / J_2 \tag{2.4}$$

where D_2^p is the second invariant of the deformation rate tensor.

A key feature of Bodner's theory is that D_2^p is assumed to be a function of J_2

$$D_2^p = f(J_2) \tag{2.5}$$

so that the above F can be defined in terms of stress. The specific form chosen for Equation (2.5) was motivated by dislocation dynamics: the dislocation velocity, and thus the strain rate, is a function of stress. Equation (2.5) can be stated either in power law form [12], or in exponential form [2,3] as follows:

$$D_2^p = D_o \exp\left[-C\left(Z^2/J_2\right)^n\right] \tag{2.6}$$

where D_o, C, and n are material constants. The mathematical simplicity and clear physical meaning of Bodner's model permit the parameter Z to be interpreted as a "threshold stress" or as a hardening parameter in extensions of the theory to strain rate and strain rate history dependencies [12,13]. In recent papers [3,4], Bodner defined Z as a hardening parameter describing "the microstructural state of the material at time t" or the "stored energy of cold work", and extended the formulation to anisotropic conditions by considering Z to be a tensor.

However, some problems still remained. It was observed that correlations for Z were apparently not transferrable from one data set to another, even for

the same material. Additionally, some hardening phenomena were not properly modeled by Equation (2.6), or Equation (1.1). This may have been caused by Bodner's use of the plastic work W^p as a measure of the viscoplastic process [7,14]. However, it also seemed entirely possible that the description of Z was simply incomplete, as explained in the following paragraphs.

Recent conferences such as [15] have recognized the importance of including mathematical representations of microstructural phenomena in macroscopic constitutive equations. In particular, see the articles by Drucker, Hart, and Aifantis in [15]. However, an approach used in many current constitutive models is to minimize the number of internal state parameters. The reasons for this approach are that (1) larger numbers of parameters can lead to non-unique parameter values in benchmarking exercises, and (2) physical justifications are increasingly harder to find as the number of mathematical "free parameters" increases. Although Bodner has recently developed a tensor form of the hardening parameter Z, each element of the tensor can be interpreted as a single macroscopic state parameter expressed in terms of five empirically determined macroscopic material constants.

Consequently, some investigators have viewed the state variable method as having "reached a point of diminishing returns" [16] because of the increasing mathematical complexity required for improved predictive accuracy, and the lack of agreement concerning which state parameters are physically important and computationally useful. These difficulties arise because the various microstructural phenomena characterized by state parameters may each dominate the flow process at different stages of deformation or in different temperature regimes. This in turn may require that a new constitutive equation be developed for each regime of performance for each material, even when microstructural correlations are available over these regimes. The resulting mathematical complexity can indeed be discouraging.

Section 3 of this report describes an alternative approach to the formulation of such constitutive equations, with the intent of providing a method that will reduce the recurring developmental requirements described above, in addition to possibly improving the understanding of how microstructural evolution determines macrostructural response. These developments rely on a recently

developed form of geometry, known as fractals. A brief summary of the attributes of fractals which are of use in this work is provided in the following paragraphs.

2.2 FRACTALS

A fractal is a geometric form which possesses two important and useful attributes: noninteger dimensionality and scale invariance. These attributes may be best described by the examples shown in Figures 2.1 and 2.2. Figure 2.1 shows a fractal known as a Koch Curve as it develops during the iterative construction process. Beginning with a line of unit length (Figure 2.1a), the line is divided into b segments of equal length, and then the original line is replaced by N new segments of length 1/b, as shown in Figure 2.1b. The next iteration is shown in Figure 2.1c, where each segment is again subdivided and

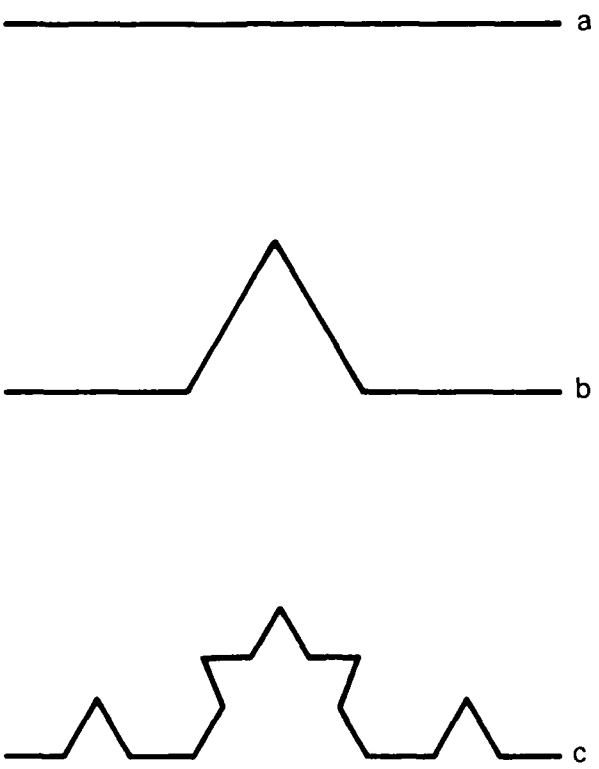

FIGURE 2.1. A Koch Curve (D=1.26)

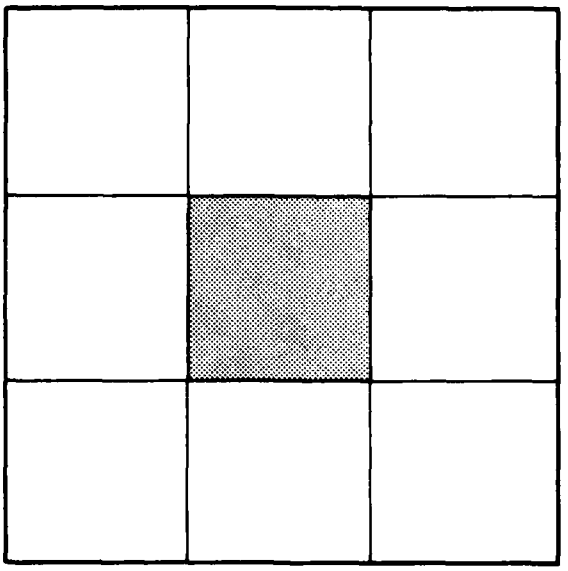

a

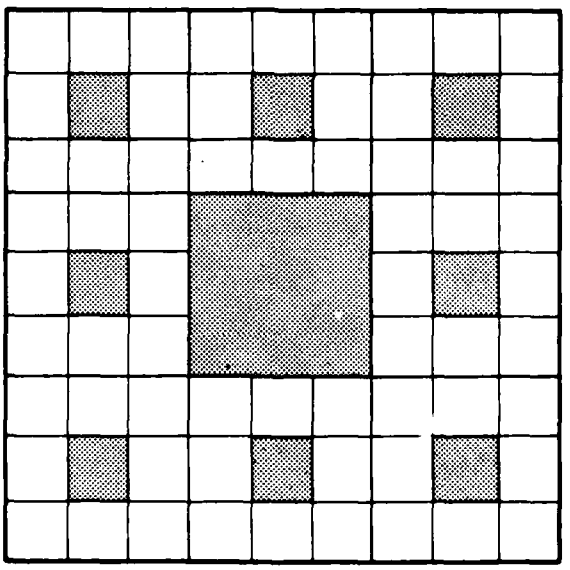

b

FIGURE 2.2. A Sierpinski Carpet (D=1.89)

replaced by N new segments. As this process continues indefinitely, the fractal develops scale invariance. That is, the fractal has the same appearance under any magnification.

The fractal dimension is defined rigorously in [8] using topological arguments. For the present purposes, computation of the fractal dimension can be briefly described as follows:

$$b^D = N \tag{2.7}$$

This means that the basic scaling unit raised to the power of the dimension is equal to the number of new units (segments). In Figure 2.1, b=3 and N=4, so that the fractal dimension of that particular curve is $D = \ln(4)/\ln(3) = 1.26$. The result is that the Koch Curve is neither a line nor a plane, but is somewhere in between. In essence, this fractal dimension describes how much space the curve fills in following its meandering course.

A second example, known as a Sierpinski Carpet, is shown in Figure 2.2. In this case, a square is divided into b=3 segments on each side, resulting in nine subsquares. Then l=1 subsquare is removed. The removed subsquare is called a "tremma", and it creates empty space in the fractal, which is called "lacunarity" [8], a term apparently originating from the description of cloud structures in meteorology. Figure 2.2b shows the Sierpinski Carpet at the second stage of construction. When this process is repeated indefinitely, the fractal again becomes scale invariant. In this case, the fractal dimension must be clarified: b^D = the number of remaining new units, which is $b^2 - l^2$, so the fractal dimension of this particular Sierpinski Carpet is

$$D = \ln(b^2-l^2)/\ln(b) = 1.89 \tag{2.8}$$

Three items are worth noting. First, fractals can be easily extended to higher dimensions. For example, the Sierpinski Carpet embedded in Euclidean 3-space becomes a Sierpinski Sponge [8] with dimension between 2 and 3. Second, for the purposes of this work, it is convenient to recognize that

fractals can be constructed by either adding or subtracting substructures, which results in the fractal dimension being either greater than or less than the dimension of the Euclidean space in which it is embedded. This feature will be of use in later discussions concerning the differences between deformation and damage. The third item is a matter of nomenclature. When a fractal is iterated a finite number of times, it is called a fractal lattice. On such a lattice, scale invariance is valid only between the two extreme characteristic lengths, and the fractal dimension is approximate [8].

The use of fractal concepts to incorporate microstructural models into Bodner's constitutive equation is described in the next section.

3.0 A MICROSTRUCTURAL FORM OF BODNER'S EQUATION

The objective of this section is to develop and verify a new form of Bodner's Equation with improved capabilities for modeling the hardening behavior of viscoplastically deforming materials. It was believed that such improvements could be obtained by incorporating microstructural information into Bodner's constitutive equation. In this manner, Bodner's continuum representation could benefit from the numerous results of metallurgical research. Because of the difficulties associated with the state variable method (see Section 2.1), an alternative approach was taken to accomplish this task. The basic concept was as follows. It has been observed that new substructures of (apparently) increasing complexity are created as materials deform viscoplastically. This is somewhat analogous to the construction process for a fractal, as outlined in Section 2.2. It was believed that the scaling properties (self-similarity) of fractals could be advantageously employed to relate the observed microstructural forms to macroscopic performance variables. Persuit of this approach led to the replacement of Bodner's empirical Z and n by known metallurgical formulas describing microstructural evolution. This new constitutive form was expected to exhibit improved hardening capabilities, thus accomplishing the above objective.

The outline of this section is as follows. The hardness/stress ratio of Bodner's Equation was interpreted as a ratio of potential gradients per unit volume. Fractal scaling concepts were then employed to render the stress equal on all scales, thus establishing local behavior with respect to scale. This in turn permitted an expansion of the above potential ratio, resulting in Bodner's Equation expressed as a product of microstructural flow resistance contributions. An approximation of this expanded form in terms of fractal structures then produced a constitutive equation explicit in scale-dependent microstructural quantities such as numbers or densities of atomic bonds, dislocations, cells, and grains. The above arguments also revealed that the power law exponent, usually found empirically, could be defined from products of known microstructural models.

An example application of this new constitutive form to the creep of a 20%Cr-35%Ni steel alloy provided limited proof that the methodology was valid.

3.1 DEVELOPMENT

The constitutive developments begin with a particular form of Bodner's Equation that separates out the hardness/stress ratio. For uniaxial loading, this form is:

$$-C \ln(\dot{\varepsilon}_s/\dot{\varepsilon}_o) = (Z/\sigma_s)^n \tag{3.1}$$

where $\dot{\varepsilon}_s$ = macroscopic plastic strain rate, $\dot{\varepsilon}_o$ = limiting strain rate in shear, C = a constant, σ_s = macroscopic stress, Z is a hardness parameter representing the "stored energy of cold work" [4,5], and n is an empirically determined exponent. Note that the left side of Equation (3.1) is a representation of a flow rate ratio and the right side is a representation of a potential ratio. Both Z and σ_s have units of stress, which is energy E (or potential) per unit volume V. Flow rates are frequently expressed as functions of potential gradients [17,18], and it is postulated that the right side of Equation (3.1) can be written as:

$$\left(\frac{Z}{\sigma_s}\right)^n = \frac{\dot{\sigma}_a}{\dot{\sigma}_s} \tag{3.2}$$

where σ_a is a potential per unit volume on the atomic scale because all deformation ultimately involves atomic bond stretching or breaking.

For each scale i, the stress is

$$\sigma_i = \frac{E_i}{V_i} = \frac{E_i}{D_i L_i} \tag{3.3}$$

where
$$V_i = L_i^{D_i} \tag{3.4}$$

L_i is a characteristic length and D_i is the fractal dimensionality. The fractal volumes serve as scaling factors for the stresses. Proper (but unknown) choices of V_i will render the stress invariant with respect to scale. That is, any arbitrarily chosen subsample of size between L_a and L_s will have the same stress, as in a true continuum. Note that although $\sigma_i/\sigma_j = 1$ for any i,j, it is not necessarily true that $\dot{\sigma}_i/\dot{\sigma}_j = 1$.

The above condition essentially establishes local behavior with respect to scale, similar to local behavior with respect to space [19-22]. Mathematically, scale invariant local behavior can be expressed as (see Discussion)

$$\sigma_a = f(\sigma_d(\sigma_c(\sigma_g(\sigma_s)))) \tag{3.5}$$

where d,c,g are the dislocation, cell and grain scales, respectively. Other scales are also possible. Then applying the chain rule to Equation (3.2) yields the product form:

$$-C\ \ell n(\dot{\varepsilon}_s/\dot{\varepsilon}_o) = \frac{\partial\sigma_a}{\partial\sigma_d}\frac{\partial\sigma_d}{\partial\sigma_c}\frac{\partial\sigma_c}{\partial\sigma_g}\frac{\partial\sigma_g}{\partial\sigma_s} = \prod_i (\dot{\sigma}_i/\dot{\sigma}_{i+1}) \tag{3.6}$$

where i = a,d,c,g and Π is the product operator. Nonlocal behavior would be manifested as additive terms in Equation (3.6) via the chain rule.

The last term of Equation (3.6) can be expanded using Equation (3.3):

$$\dot{\sigma}_i/\dot{\sigma}_{i+1} = \frac{V_{i+1}}{V_i}\frac{\dot{E}_i - \sigma_i\dot{V}_i}{\dot{E}_{i+1} - \sigma_{i+1}\dot{V}_{i+1}} \tag{3.7}$$

Each of the V_i in Equation (3.7) contains a fractal dimensionality D_i. It is natural to assume that D changes with both scale and deformation. However, the D's are assumed unknown in the present development, and will be eliminated with the approximation shown by the dashed lines in Figure 3.1, as follows. First, substitution of Equations (3.7) into (3.6) yields, after cancellations,

$$-C \ln(\dot{\varepsilon}_s/\dot{\varepsilon}_o) = \left(\frac{\dot{E}_a - \sigma_a \dot{V}_a}{\dot{E}_s - \sigma_s \dot{V}_s}\right) \prod_j \left(\frac{L_{i+1}}{L_i}\right)^{D_j} \tag{3.8}$$

where i = a,d,c,g, and the subscript j is defined in Figure 3.1. Note that Equation (3.8) contains products of lengths of powers (local), rather than a sum of lengths to powers (nonlocal) as suggested in [23]. Second, the characteristic lengths L_i may be expressed in a standard form by scaling upward from the characteristic length of the atomic scale, $L_a = a_o$, an appropriate lattice constant. Using the scaling parameter (b) of Equation (2.7), we have

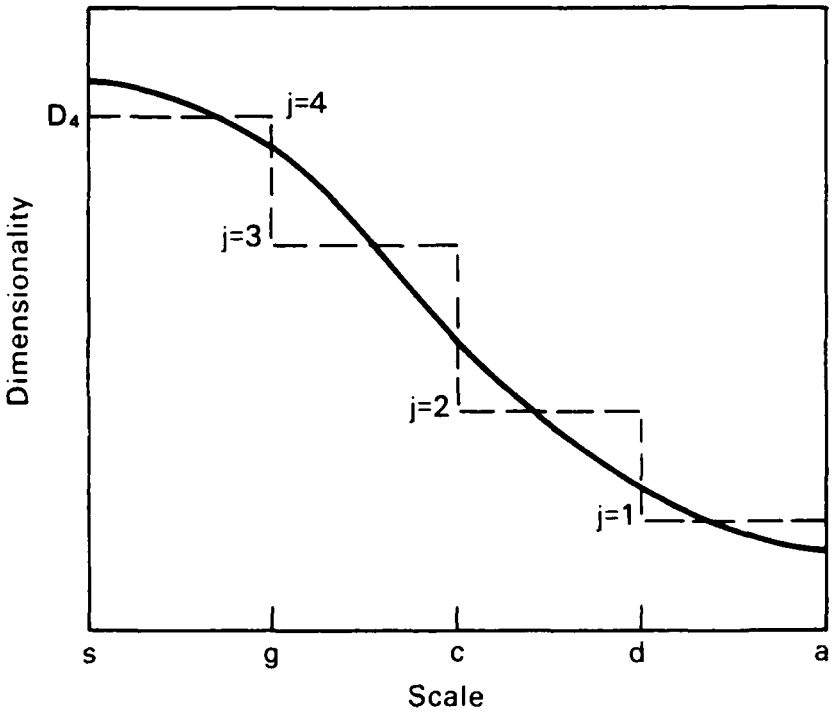

FIGURE 3.1. Conceptual Diagram for Dimensionality as a Function of Scale

$$L_i = a_o \, b^{m_i} \tag{3.9}$$

where m_i is the number of fractal construction iterations required to scale from the atomic to the ith scale. Consequently, the length ratios in Equation (3.8) can be written

$$(L_{i+1}/L_i)^{D_j} = b^{\Delta m_j D_j} \tag{3.10}$$

where Δm_j is the number of iterations between scales i and i+1. Lastly, substituting Equations (2.7) and (3.10) into (3.8) eliminates the D's if b is held constant over all scales, yielding

$$-C \, \ell n(\dot{\varepsilon}_s/\dot{\varepsilon}_o) = \left(\frac{\dot{E}_a - \sigma_a \dot{V}_a}{\dot{E}_s - \sigma_s \dot{V}_s}\right) \prod_j (N_j^{\Delta m_j}) \tag{3.11}$$

where $N_j^{\Delta m_j}$ is the total number of new fractal structure subunits introduced in iterating from scale i to i+1. These N-terms represent microstructural features such as the number of atoms per dislocation or the number of dislocations per dislocation cell.

Additional approximations reduce this constitutive equation to a simpler form. The terms $\dot{V}_i$ represent the rates of volumetric change, and can be set to zero by virtue of the first strain invariant (ε_{ii}=0), a frequent assumption employed in non-elastic analyses. Expressing E_s as the plastic work yields $\dot{E}_s = \tau_s \dot{\varepsilon}_s$, where $\tau_s = \phi\sigma_s$ and ϕ is the Schmid factor. On the atomic scale, $\dot{E}_a = F_a v_a$, and the separation force can be approximated as $F_a = \Delta E_a/\Delta x_a = E_o/a_o$, where E_o is the atomic binding energy. The velocity v_a can be assumed equal to the average velocity of mobile dislocations v_m. Substitution of these approximations into Equation (3.11) yields, after rearranging:

$$\dot{\varepsilon}_s = \dot{\varepsilon}_o \exp\left[-\left(\frac{CE_o v_m}{a_o \phi \sigma_s \dot{\varepsilon}_s}\right) \prod_j (N_j^{\Delta m_j})\right] \tag{3.12}$$

The exponent in Equation (3.12) has essentially been separated into the form: (Physics Data)/Engineering Data) x (Metallurgical Models), where "Physics Data" represents known quantities on the atomic scale, "Engineering Data" represents known measurables on the macroscopic sample scale, and "Metallurgical Models" represents microstructural phenomena on intermediate scales. If the microstructural phenomena controlling the deformation rate are known, models from the metallurgical literature may be substituted for the N-terms. Different substitutions can be made as the controlling microstructure evolves with deformation or temperature. Equation (3.12) thus provides a flexible methodology for incorporating microstructural information into macroscopic constitutive equations.

3.2 APPLICATION

Limited verification of Equation (3.12) was obtained by simulating the hardening behavior for a 20%Cr-35%Ni steel undergoing a normal creep transient and entering the steady state creep regime at 700°C [24,25,26], as follows. First, the dislocation velocity v_m in Equation (3.12) was related to the macroscopic strain rate by the Orowan equation, $\dot{\varepsilon}_s = B\rho_m v_m$, where B is the Burger's vector and ρ_m is the density of mobile dislocations (cm^{-2}). This cancelled $\dot{\varepsilon}_s$ from the right side of Equation (3.12). Only atomic and dislocation N-terms were employed in this first approximation, and both were assumed to represent stored energies, consistent with the definition of Z [5]. $N_1^{\Delta m_1}$ represented the number of atomic bonds left in a strained condition after a dislocation loop expands to a typical radius proportional to the total dislocation density, $r = \rho_T^{-1/2}$ [25]:

$$N_1^{\Delta m_1} = 2\pi/(a_o \rho_T^{1/2}) \qquad (3.13)$$

The second microstructural term represented the energy storage at the dislocation scale, and was defined as the number of immobile dislocations per square cm of sample area:

$$N_2^{\Delta m_2} = \rho_I \tag{3.14}$$

Substituting the above microstructural models into Equation (3.12) gave

$$\dot{\varepsilon}_s = \dot{\varepsilon}_o \exp\left(-\frac{2\pi C E_o \rho_I}{a_o^2 B \phi \sigma_s \rho_m \rho_T^{1/2}}\right) \tag{3.15}$$

The constitutive equation was then expressed in terms of only the total dislocation density ρ_T, a more desirable state parameter [11], by employing the dislocation distribution models in [27]:

$$\rho_m/\rho_T = \exp(-k\Theta) \sum_{r=0}^{k} \frac{(k\Theta)^{k-r}}{(k-r)!} \tag{3.16}$$

$$\rho_I = \rho_T - \rho_m \tag{3.17}$$

where $\theta = GB\rho_T^{1/2}/\tau_s$, G is the shear modulus, and k is an integer describing the "sharpness" of the distribution [27]. Substituting Equations (3.16) and (3.17) into (3.15) gave

$$\dot{\varepsilon}_s = \dot{\varepsilon}_o \exp\left(-\frac{2\pi C E_o}{a_o^2 B \phi \sigma_s \rho_T^{1/2}} \frac{1-f}{f}\right) \tag{3.18}$$

where f is defined by the right hand side of Equation (3.16). Estimated values for the above material parameters are [25,26,28]: $\dot{\varepsilon}_o = 3.13 \times 10^{-5}$/sec, E_o = 4.29 eV/atom at 0°K, $a_o = 2.86 \times 10^{-8}$ cm, $B = 2.5 \times 10^{-8}$ cm, $G = 7.3 \times 10^5$ kg/cm^2, $\phi = 1/3.1$. The constant C was taken as unity, and k in Equation (3.16) was set equal to 4 based on observation of the dislocation distributions in [26] compared to those in [27].

Equation (3.18) was tested in the following manner. The macroscopic creep rate for Fe-20%/Cr-35%Ni at 700°C and 1300 kg/cm^2 was determined graphically from Fig. 2 of [25], and was used as input to solve iteratively for the corresponding ρ_T versus time. The results are shown in Figure 3.2, along with

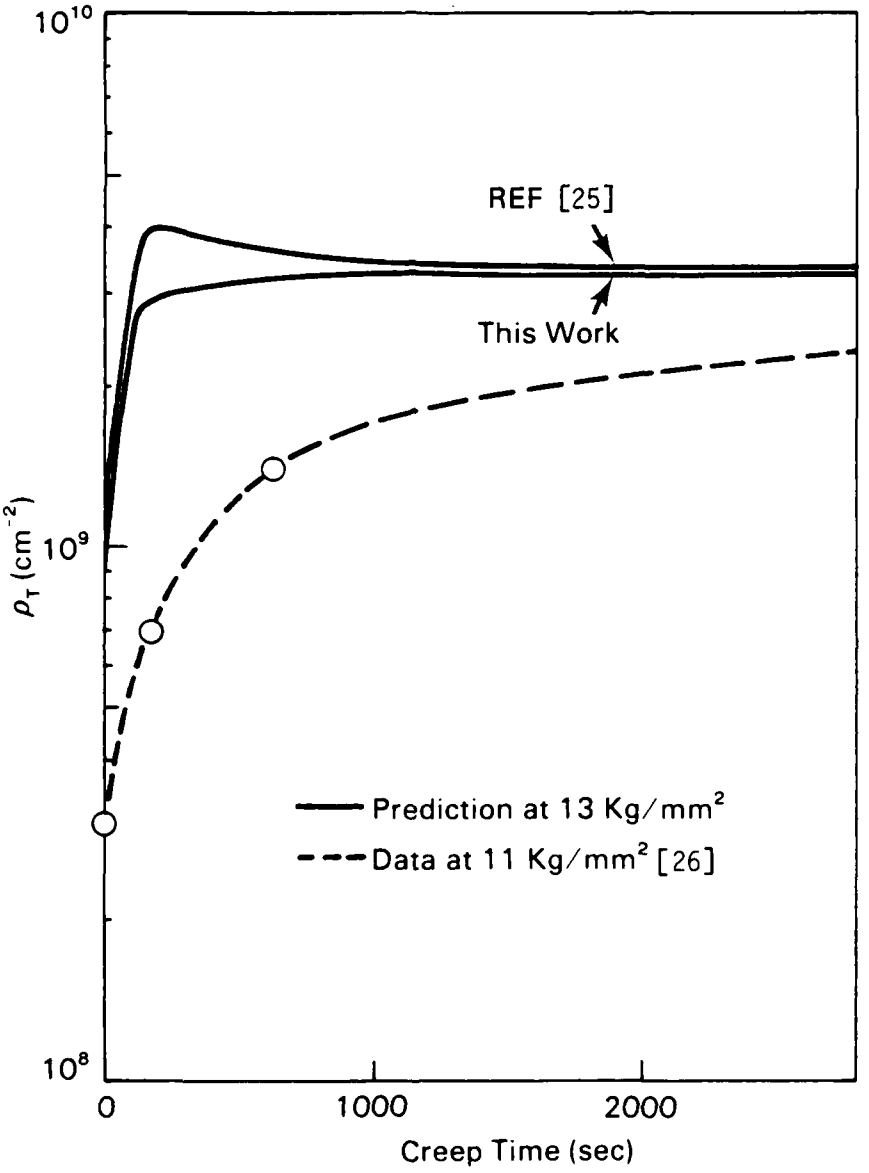

FIGURE 3.2. Predicted and Measured Total Dislocation Densities for Fe-20%Cr-35%Ni at 700°C

another prediction from [25], and data at an applied stress of 1100 kg/cm^2 [26]. Unfortunately, data at 1300 kg/cm^2 were not available for comparison. However, Figure 3.2 shows reasonably good quantitative agreement with the prediction of [25] at 1300 kg/cm^2, which required three adjustable parameters and reproduced the creep history rather well. Although the qualitative agreement with the data at the lower stress is acceptable, improvements are possible by decreasing k and adjusting ρ_T as the time approaches zero. The "softer" distribution at lower strains (shorter times) is also documented in [26].

The above results are subject to errors originating from the graphical interpretation of $\dot{\varepsilon}_s$, the approximation in Figure 3.1, and the approximation that microstructural phenomena on scales larger than dislocations were negligible. However, the reasonably good results can be taken as an indication that the above developments are valid and useful constitutive forms.

3.3 DISCUSSION

The state variable approach to devleloping viscoplastic constitutive equations is a valuable method because it has the capability of combining models from both continuum mechanics and metallurgy, resulting in a pragmatic use of available information. However, the resulting complexity of the mathematical expressions is sometimes a disadvantage, and the physical meaning of the correlations is not always clear. This section has attempted to address these problems by restating Bodner's macroscopic constitutive equation in a form that readily admits microstructural concepts.

A number of qualifying statements are in order. First, the power law form chosen as the starting point of this development [Equation (1.1)] limits the present results to uniaxial loading conditions. Multiaxial and anisotropic forms of Bodner's law are available in [4]. The hardness/stress ratio of Equation (3.1) results in the N-terms being defined as flow resistance or energy storage contributions, whereas other ratios may require different definitions.

Second, there is currently no proof that Equation (3.2) is true, although the validity of the resulting constitutive development is supported by the example application described above. Further testing is needed for a variety of materials and conditions. Additional work is also needed to confirm the

following observation: the expanded form in Equation (3.6) implies that the empirical power law exponent (n) effectively originates from the product of microstructural flow resistance contributions on various scales within the material. A physical interpretation is that the N-terms (microstructural models) are commonly expressed as functions of σ_s to rational powers p in the metallurgical literature. After taking the derivatives in Equation (3.6), n effectively becomes a sum of p's. Because various microstructural phenomena dominate at various stages of deformation, this could possibly explain why n frequently assumes non-interger values that change with deformation. Nonlocal behavior could result in a more complicated $n = f(p)$.

Third, the time derivatives in Equation (3.2) may raise questions related to Prager's consistency condition [19]. This form was postulated in order to eliminate the plastic work integral, which is an "undesirable" state variable [7,11]. Although other gradients may be possible, the present approach facilitates simplification of the right hand side of Equation (3.11) by metallurgical rate laws and the conservation of volume.

Fourth, many fractals lack translational invariance (i.e., p. 426 of [8]), which conflicts with the fundamental postulate of frame indifference in continuum mechanics. However, the fractal scalings render the material behavior local with respect to scale, thus imposing a condition similar to a "true continuum" (i.e., a fluid) which possesses such invariance. Additionally, many useful constitutive theories violate this postulate [19], so the question may be irrevelant in practice.

This problem can also be addressed by an alternative approach which has been successful in solid state physics [i.e., 29]. That approach is to consider the viscoplastic deformation process to occur on fractal lattices, or in "fractal space," as follows. The potentials (E) in Equation (3.3) contain only the fundamental quantities of force and length, which are invariant with respect to transformations from Euclidean to fractal space. However, the volume terms contain the dimensionality (D), which can only assume integer values in Euclidean space. Recognition of D as another fundamental quantity that can assume non-integer values requires the proper space for representation. The above constitutive form can be developed by employing fractal space,

and assuming that Z/σ appears as a potential gradient there, as in the central terms of Equation (3.6). Interpretation of these gradients ($\partial\sigma_i/\partial\sigma_j$) as measures of energy transfer from one scale to the next naturally leads one to expect local behavior with respect to scale, because relations between remote scales would not be expected to be significant on physical grounds. For example, atomic bond breaking would have a greater effect on dislocation dynamics than on grain size. In any case, the number of terms in the chain rule expansion can easily be chosen to enforce local behavior. The result is that the chain rule, which is still valid in fractal space [29], again produces the product form of Equation (3.6). The key assumption concerns the existence of the potential gradient in fractal space, and the key result is the "continuization" of the stress to produce local behavior as viewed from fractal space.

In conclusion, the above constitutive form does not provide any new information about microstructural models per se. However, it does appear to provide a useful methodology for incorporating those models into macroscopic constitutive equations, and a physical description for the origin of the power law exponent. The results of these developments are expected to be manifested as improvements in the ability of Bodner's constitutive equation to model the hardening behavior of engineering metals and alloys.

4.0 PROGRESS TOWARD A COMBINED HARDENING/DAMAGE STATE TENSOR

The developments in Section 3 employed an approximation of the scale-dependent fractal dimensionality (D) (Figure 3.1) in order to express Bodner's Equation in terms of microstructural models. Although the above results are useful, as outlined in the Summary, it was thought that a constitutive equation addressing both hardening and damage could be obtained without having to incorporate specific metallurgical models. In essence, the microstructural phenomena would be implicit in the constitutive formulation, which in turn would be a function of only well-known data on the atomic scale (i.e., atomic binding energy) and the macroscopic state variables (i.e., strain and stress). The initial point of departure for this attempt was Bodner's Equation in the form (see Equation (3.8)).

$$-C \ln \left(\dot{\varepsilon}_s / \dot{\varepsilon}_o\right) = \frac{\dot{E}_a}{\dot{E}_s} \frac{L_s{}^{D_s}}{L_a{}^{D_a}} \tag{4.1}$$

With characteristic lengths and energies comparatively well known, the problem was to find solutions for the dimensionalities in Equation (4.1) in terms of only the macrostructural state variables (ε_s, $\dot{\varepsilon}_s$, σ_s). If increases or decreases in the D's were assumed to represent hardening or damage, respectively, these solutions could then be used to define a combined hardening/damage state tensor. An unsuccessful attempt to find these solutions for the uniaxial isotropic case by analysis of the conservation of mass equation is described briefly in the Appendix.

A second attempt was successful. Concepts from the nonclassical, or "nonlocal," continuum theories [20-22, 30-35] were found to provide a framework useful to accomplish the second objective in the Summary. The central idea was that the hardening and damage substructures act as inhomogeneities that cause fluctuations in the internal stress fields, or the "stress polarization" depicted in Figure 4.1. The problem was thus redefined to be the development

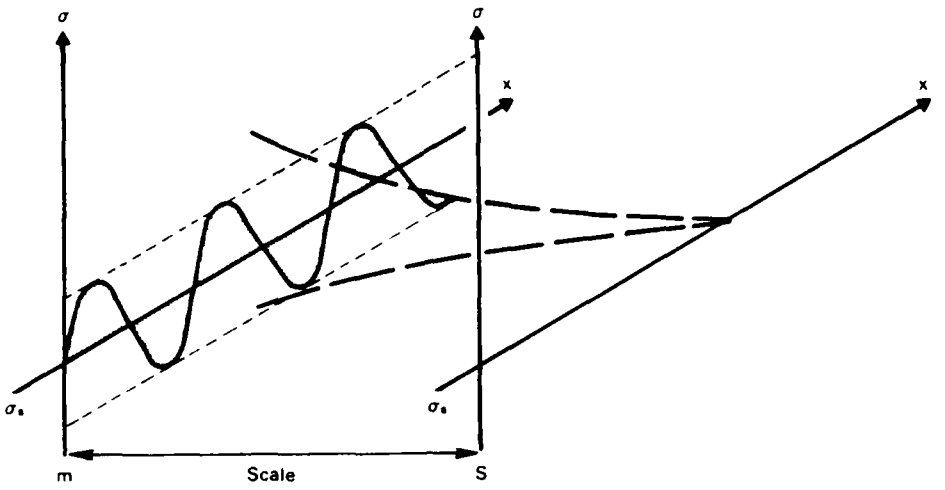

FIGURE 4.1. Stress Polarization as a Function of Scale

of a scale-dependent viscoplastic stress polarization equation and its solution as a function of suitable hardening and damage state parameters.

The general approach was as follows. As in Section 3, the hardness/stress ratio was represented by a ratio of potential gradients, except that nonlocal behavior was permitted by letting the numerator represent the scale at which the microstructure controls the strain rate. This was used to develop a relation between the energy storage rates for the controlling and macroscopic scales. Fractal scaling concepts were then employed to define the scale factor for the above relation in terms of hardening and damage. Definition of a strain rate scaling equation then resulted in scale invariance of the energy storage rate, with respect to the strain on each scale. Stored energies were defined in terms of effective moduli on each scale, and the stress polarization equation was produced by rearrangement of the above scale invariant storage rate equation. Embedded within the polarization equation is a function describing the combined hardening/damage state in terms of departures from unity, thus providing the basis for the desired new state tensor. The above developments are described in more detail in the next subsection, followed by preliminary verification results.

4.1 A STRESS POLARIZATION EQUATION FOR VISCOPLASTICITY

A key requirement for expression of the stress polarization equation is the following scale invariant energy storage rate equation

$$\frac{dU_s}{d\varepsilon_s} = \frac{dU_m}{d\varepsilon_m} \tag{4.2}$$

Although this equation could probably have been simply assumed by virtue of the "fractal space" arguments in Section 3.3, the following derivation is presented to place the polarization equation on a firmer foundation.

4.1.1 An Energy Storage Rate Scaling Equation

Arguments begin from the same starting point as did the microstructural developments in Section 3 of this report. Bodner's Equation is stated in the form

$$-C\ \ell n(\dot{\varepsilon}_s/\dot{\varepsilon}_o) = \left(\frac{Z}{\sigma_s}\right)^n \tag{4.3}$$

where the subscript s denotes the sample scale, Z is the hardening parameter which represents the storage of cold work, and n is the empirical exponent. It is again assumed that the hardness/stress ratio on the right hand side of the above equation can be expressed as a ratio of potential gradients:

$$\left(\frac{Z}{\sigma_s}\right)^n = \frac{\partial\sigma_m}{\partial\sigma_s} = \frac{\dot{\sigma}_m}{\dot{\sigma}_s} \tag{4.4}$$

However, in this case it is assumed that the potential σ_m occurs on the scale m at which the microstructure is controlling the deformation rate $\dot{\varepsilon}_s$ at a particular macroscopic state of the material (ε_s, σ_s). In essence, m represents the scale at which a nonlocal theory is required to describe the internal

stress field fluctuations caused by hardening or damage inhomogeneties. Above this scale, local theories would suffice. It is assumed that the scale m can change as the material state changes, i.e., as deformation advances.

As before, each potential is expressed as the ratio of a characteristic energy over a characteristic volume

$$\sigma_i = E_i/V_i \tag{4.5}$$

where the volume on scale i is a fractal volume denoted by

$$V_i = L_i^{D_i} \tag{4.6}$$

and L_i is the characteristic length of scale i. Substituting Equation (4.5) into Equation (4.4) and performing the differentiations, Equation (4.3) can be written as

$$-C\ \ell n(\dot{\varepsilon}_s/\dot{\varepsilon}_o) = \frac{\dot{E}_m - \sigma_m \dot{V}_m}{\dot{E}_s - \sigma_s \dot{V}_s}\left(\frac{V_s}{V_m}\right) \tag{4.7}$$

where the $(\dot{})$ denotes time differentiation. Note that because the chain rule was not employed and differentiation was performed independently for the numerator and denominator, it is not necessary to assume local behavior with respect to scale.

The term $\dot{E}_m$ in the numerator represents the rate of energy storage by microstructural features on scale m, a generalization of the results in [34], and is hereafter denoted $\dot{U}_m$ for clarity. The $\dot{E}_s$ term in the denominator represents the rate at which plastic work is performed by the effective stress $\Psi\sigma_s$, where Ψ denotes the Schmid factor. The denominator is expressed hereafter as $\dot{W}_s = \Psi\sigma_s\dot{\varepsilon}_s$ for clarity.

As before, the first strain invariant is assumed to be zero (Tr $\varepsilon = 0$) on all scales, which results in volume conservation, so that the $\dot{V}$ terms in Equation (4.7) vanish. When the above substitutions and Equation (4.6) are inserted into Equation (4.7), the result after some minor manipulations is

$$(\Psi\sigma_s\dot{\varepsilon}_s)\,[C\ \ln(\dot{\varepsilon}_o/\dot{\varepsilon}_s)] = \dot{U}_m\left(\frac{L_s^{D_s}}{L_m^{D_m}}\right) \tag{4.8}$$

This equation is interpreted to mean that the rate of plastic work on the macroscopic scale (s) times a rate factor equals the rate of energy storage on another scale (m<s) times a scale factor. In essence, the same result found in [34] has been expanded to include both rate and scale dependence. This is valid for any scale, so setting m=s in Equation (4.8) gives

$$(\Psi\sigma_s\dot{\varepsilon}_s)\,[C\ \ln(\dot{\varepsilon}_o/\dot{\varepsilon}_s)] = \dot{U}_s \tag{4.9}$$

which means that the rate of macroscopic plastic work times the rate factor equals the rate of macroscopic energy storage. This result seems reasonable, so that combining the last two equations produces

$$\dot{U}_s = \dot{U}_m\left(\frac{L_s^{D_s}}{L_m^{D_m}}\right) \tag{4.10}$$

which relates the macroscopic energy storage rate to that on any other scale. This equation indicates that energy storage rate (flow resistance) contributions from different scales are indeed different, and require quantification by the N-terms in Section 3 when incorporated into Bodner's Equation. When the $\dot{\varepsilon}_s$ of Equations (4.8) and (4.9) is retained, a more useful form of Equation (4.10) is produced

$$\frac{dU_s}{d\varepsilon_s} = \frac{dU_m}{d\varepsilon_s}\left(\frac{L_s^{D_s}}{L_m^{D_m}}\right) \tag{4.11}$$

4.1.2 Definition of the Scale Factors

The next step in the development of the scale and rate dependent stress polarization equation concerns the definition of the scaling factor in parentheses in Equation (4.11). This definition requires the introduction of some rather general fractal arguments, as follows. It is assumed that the relationship between the structural characteristics on scales m and s can be represented by a single, or a finite number of, iterative fractal construction steps. The fractal may extend to scales larger than s or smaller than m, so it represents a "covering" or "overlay" onto the material's structural features at those scales. Further, a different fractal may be employed for this "overlay" for each state of the system (ε_s, σ_s), which permits the ratio of characteristic lengths L_s/L_m to change as deformation advances. The only restriction on the fractal is that the dimensionalities (D) at scales m and s be equal, so that Equation (4.11) becomes

$$\frac{dU_s}{d\varepsilon_s} = \frac{dU_m}{d\varepsilon_s}\left(\frac{L_s}{L_m}\right)^D \tag{4.12}$$

Next, the scale factor b_m is defined as

$$b_m = L_s/L_m \tag{4.13}$$

where the characteristic lengths L_s and L_m represent the strained condition on each scale, consistent with the above description. The relation $b^D = N$ is valid for any fractal description, although only approximately for a finite number of fractal construction iterations, i.e., a fractal lattice. Substitution of this relation and Equation (4.13) into Equation (4.12) yields

$$\frac{dU_s}{d\varepsilon_s} = N_m \frac{dU_m}{d\varepsilon_s} \tag{4.14}$$

where N_m is defined as the number of new substructural units remaining after the fractal iteration (see Section 2.2). This is related to hardening and damage as follows.

The creation or annihilation of hardening or damage substructures as deformation advances can be viewed as modifications in the fractal construction process. Schematically, this is shown in Figure 4.2. On the scale s, the characteristic length L_s is described by the true strain ε_s

$$L_s = L_{so}\, e^{\varepsilon_s} \tag{4.15}$$

where $L_{so} = L_s(\varepsilon_s = o)$. On scale m, the same total length L_s is made up of N_m units of initial length L_{so}/b_m, which are each strained by ε_m

$$L_s = \left(\frac{L_{so}}{b_m}\, e^{\varepsilon_m}\right) N_m \tag{4.16}$$

The term in parentheses is L_m, analogous to L_s in Equation (4.15). The term N_m can be represented as a departure from the homogeneous condition, which is specified by $N_m = b_m = 3$ in Figure 4.2. In the homogeneous case, the line on the s scale remains a line on the m scale, as shown by the dimensionality $D_m = \ell n N_m / \ell n b_m = \ell n b_m / \ell n b_m = 1$. In the hardening case, extra subunits are introduced, so that $N_m > b_m$ and $D_m > 1$. The three-sided "box" in the lower left hand side of Figure 4.2 represents a hardening structure such as a dislocation tangle or a cell wall, each of which effectively increases the magnitude of the energetic path for the passage of another dislocation from point A to B. Conversely, the open section at scale m in the lower right hand side of the figure represents a void or other similar structure which decreases the resistance for subsequent deformation.

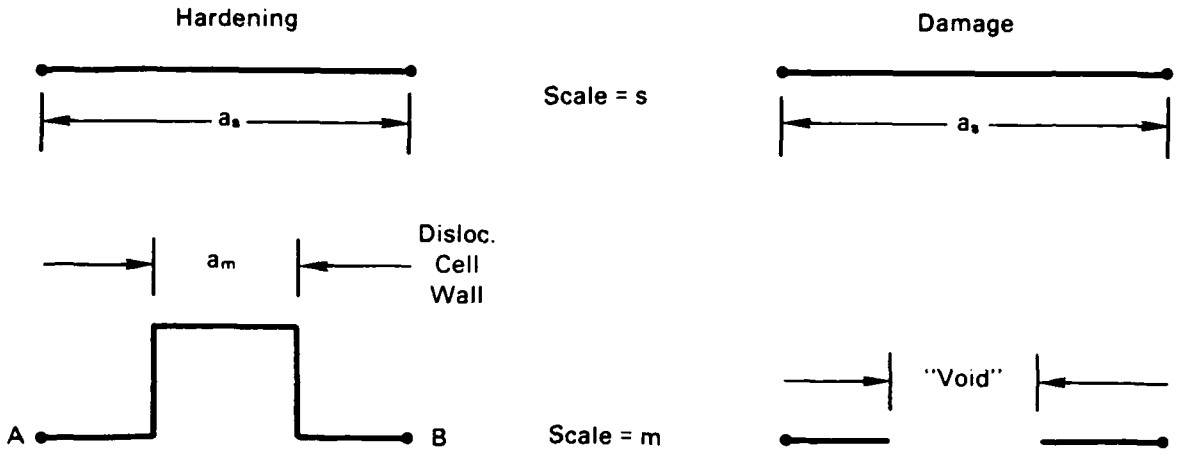

FIGURE 4.2. Hardening and Damage Defined by Simple Fractal Models, with $b_m = 3$

N_m was defined simply as

$$N_m = r_m b_m \tag{4.17}$$

where $r_m > 1$ for domination by hardening and $r_m < 1$ for domination by damage (softening).

4.1.3 Scale Invariance of Energy Storage Rate

Substitution of Equation (4.17) into (4.14) gives

$$\frac{dU_s}{d\varepsilon_s} = r_m b_m \frac{dU_m}{d\varepsilon_s} \tag{4.18}$$

The derivative on the right hand side of Equation (4.18) is considered unknown, a condition remedied by the following change of variables:

$$\frac{dU_m}{d\varepsilon_s} = \frac{dU_m}{d\varepsilon_m} \frac{d\varepsilon_m}{d\varepsilon_s} \tag{4.19}$$

Insertion of this equation into Equation (4.18) reveals that definition of the strain rate scaling relation

$$\frac{d\varepsilon_m}{d\varepsilon_s} = \frac{1}{r_m b_m} \tag{4.20}$$

leaves the stored energy invariant with respect to the strain on each scale

$$\frac{dU_s}{d\varepsilon_s} = \frac{dU_m}{d\varepsilon_m} \tag{4.21}$$

This is the key relation needed for development of the stress polarization equation. Note the similarity to the scale invariant stress of Section 3 under linear elastic conditions.

4.1.4 The Polarization Equation

Development of the stress polarization equation eventually requires that the energy storage rate terms above be expressed in terms of effective moduli so that the path-dependent DEM formulations in [10] can be employed. This is accomplished as follows. For any sale, the energy terms (U) can be expressed in the following form, where subscripts represent principal axes:

$$U = 1/2\ \lambda\ (\gamma_{ij})^2 + G(\gamma_{jj}^2) + 1/2\ G(\gamma_{ij}{}^2) \tag{4.22}$$

where λ is Lame's constant, G is the shear modulus, and the last term in parentheses above represents the sum of squares of shear strains. Because $Tr\varepsilon = 0$ has already been assumed, differentiation of Equation (4.22) by the principal strains ε gives

$$\frac{dU_i}{d\varepsilon_i} = 2G_i\varepsilon_i + \frac{dG_i}{d\varepsilon_i}\ \varepsilon_i{}^2 \tag{4.23}$$

for any scale i. Substitution of this equation into Equation (4.21) and employing the relation $2G_i\varepsilon_i = \sigma_i/(1+\nu_i)$ gives

$$\frac{dG_s}{d\varepsilon_s}\varepsilon_s^2 + \frac{\sigma_s}{1+\nu_s} = \frac{dG_m}{d\varepsilon_m}\varepsilon_m^2 + \frac{\sigma_m}{1+\nu_m} \tag{4.24}$$

where ν is Poisson's ratio, which is dependent on the dimensionality D_i as follows [36]

$$\nu_i = \frac{6-D_i}{12+D_i} \tag{4.25}$$

However, $D_s = D_m = D$, so $\nu_s = \nu_m = \nu$. Rearranging Equation (4.24) gives

$$\sigma_s - \sigma_m = (1+\nu)\left(\frac{dG_m}{d\varepsilon_m}\varepsilon_m^2 - \frac{dG_s}{d\varepsilon_s}\varepsilon_s^2\right) \tag{4.26}$$

But by Equation (4.9)

$$\frac{dG_s}{d\varepsilon_s}\varepsilon_s^2 = \sigma_s\left[C\Psi\,\ell n(\dot{\varepsilon}_o/\varepsilon_s) - \frac{1}{1+\nu}\right] \tag{4.27}$$

Definition of the stress polarization at scale m as (see Figure 4.1)

$$\sigma_{pm} = \sigma_s - \sigma_m \tag{4.28}$$

and substitution of the last two equations into Equation (4.26) gives the <u>stress polarization equation</u>

$$\sigma_{pm} = (1+\nu)\left(\frac{dG_m}{d\varepsilon_m}\varepsilon_m^2 - \sigma_s\left[C\Psi\,\ell n(\dot{\varepsilon}_o/\dot{\varepsilon}_s) - \frac{1}{1+\nu}\right]\right) \tag{4.29}$$

where the modulus term represents the rate of microstructural change on scale m, and the last bracket effectively contains only macroscopic data because ν can be approximated by the usual macroscopic constant value. This occurs

because changes in D are relatively small over most scales and strain ranges of interest, an observation made during the work described in the Appendix.

It should be noted that the spatial dependence of the internal stress fluctuations does not appear in the above polarization equation. This dependence has been absorbed into the scale factor b_m, defined in Equation (4.13). Also the "polarization" itself in Equation (4.29) represents the departure from a "true continuum," where the stresses are equal on all scales of interest, as in a fluid. Of primary interest is the envelope defined by the dashed lines in Figure 4.1, rather than the details of the waveform plotted versus the X-axis in that figure. The scale-dependent envelope of stress fluctuations, depicted by the heavy dashed curves, is actually expected to exhibit a periodic nature representative of nonlocal behavior confined to specific scale regimes by substructures of specific characteristic sizes. The solution for this envelope shape as a function of scale will yield useful information concerning substructure evolution, and is the subject of future work.

4.1.5 Path-Dependent Effective Moduli

In Equation (4.29), the rate of change of the effective modulus with respect to strain is given by the path-dependent *differential effective medium* (DEM) theory of [10]. Path dependence means that the effective modulus at any state (ε_s, σ_s) depends on the entire sequence of combinations of hardening and damage substructures that occurred to reach that state. The DEM approach describes the rate of change of the effective modulus in terms of the amount and rate of addition of these two types of inhomogeneities to a parent material. These two inhomogeneities are described in terms of their volume fractions, herein denoted ϕ_h and ϕ_d, where the subscript m has been dropped for efficiency of notation. The volume fraction of the parent material (the "backbone") is denoted ϕ_0, and it is required that

$$\phi_0 + \phi_h + \phi_d = 1 \tag{4.30}$$

The rate of change of the bulk (K) and shear (G) moduli with respect to an independent variable, denoted here by ($^\bullet$), are given by:

$$\dot{K} = (K_h - K)\, P_h \left(\dot{\phi}_h + \frac{\phi_h \dot{\phi}}{1-\phi} \right) + (K_d - K)\, P_d \left(\dot{\phi}_d + \frac{\phi_d \dot{\phi}}{1-\phi} \right) \tag{4.31}$$

$$\dot{G} = (G_h - G)\, Q_h \left(\dot{\phi}_h + \frac{\phi_h \dot{\phi}}{1-\phi} \right) + (G_d - G)\, Q_d \left(\dot{\phi}_d + \frac{\phi_d \dot{\phi}}{1-\phi} \right) \tag{4.32}$$

where $\phi = \phi_h + \phi_d$. The initial conditions are $K(0) = K_o$, $G(0) = G_o$. The P and Q above depend on the shapes of the substructures, and were selected as follows. Hardening structures were assumed to be of plate or disk form, analogous to grain boundaries, dislocation tangles, or cell walls. The moduli of the hardening structures (K_h, G_h) were thus assumed to be those representing the state of maximum hardness in the macroscopic material. The damage structures were assumed to be of a spherical void form, representing a ductile material such as aluminum. The disc shape would have introduced singularities into the formulation when the damage moduli (K_d, G_d) were assumed to be zero, as expected physically. The P and Q for hardening substructures are [10]

$$P_h = \frac{K + K_h^*}{K_h + K_h^*} \qquad Q_h = \frac{G + G_h^*}{G_h + G_h^*} \tag{4.33}$$

and for damage substructures are

$$P_d = \frac{K + K^*}{K^*} \qquad Q_d = \frac{G + G^*}{G^*}$$

where
$$K^* = 4/3\ G \qquad G^* = G/6 \left(\frac{9K + 8G}{K+2G} \right) \tag{4.34}$$

$$K_h^* = 4/3\ G_h \qquad G_h^* = G_h/6 \left(\frac{9K_h + 8G_h}{K_h + 2G_h} \right) \tag{4.35}$$

Preliminary results concerning the verification of the above scale- and rate-dependent stress polarization formulation (Equations (4.29) to (4.35)) are shown in the next subsection.

4.2 PRELIMINARY VERIFICATION RESULTS

Limited verification of the above scale- and rate-dependent stress polarization equation was obtained for the case of pure aluminum undergoing creep at 3.0 MPa and 593°K [37]. Because of the complexity of Equations (4.29) to (4.35), some simplifications were required for this effort to remain within project resources. Consequently, verification was obtained only for hardening behavior. The general approach was to introduce approximations for some of the data and terms needed for the complete solution of Equation (4.29). This equation was then rearranged so that the characteristic sizes of the controlling substructures could be predicted as a function of the macroscopic strain, and the results compared to data. This was accomplished as follows.

4.2.1 Specialization for Hardening Behavior

The following change of variable in the modulus rate term of Equation (4.29) was found to eliminate dependence on $\dot{\phi}_h$, leaving only dependence on ϕ_h:

$$\frac{dG_m}{d\varepsilon_m} = \frac{dG_m}{dr_m}\frac{dr_m}{d\varepsilon_m} \tag{4.36}$$

It was assumed that r_m was adequately approximated by

$$r_m = 1 + \phi_h - \phi_d \tag{4.37}$$

so that with $\phi_d = \dot{\phi}_d = 0$,

$$\frac{dG_m}{dr_m} = (G_h - G)\left[\frac{G+G_h^*}{G_h+G_h^*}\right]\left(\frac{1}{1-\phi_h}\right) \tag{4.38}$$

where the value of $G = f(\phi_h(\varepsilon_s))$ at the current hardened state was approximated by the larger of the Hashin-Shtrikman bounds for two-phase composites [10], consistent with domination by hardening (ϕ_d=0) and the use of the strain energy in Equation (4.22) [30,31]. Again note the dropping of the subscript m from ϕ, G_h, and G_h^* terms for ease of notation.

A representation for $dr_m/d\varepsilon_m$ was found by combining Equations (4.15) and (4.16) to give

$$\varepsilon_m = \varepsilon_s - \ell n r_m \tag{4.39}$$

which was then differentiated with respect to ε_m and combined with Equation (4.20) to yield

$$\frac{dr_m}{d\varepsilon_m} = r_m(r_m b_m - 1) \tag{4.40}$$

This equation represents the case of multiaxial deformation because the vertical segments in the lower left diagram of Figure 4.2 are allowed to strain. A uniaxial representation is also possible if Equation (4.16) is rewritten so that vertical segments do not strain:

$$L_s = \left(\frac{L_{so}}{b_m} e^{\varepsilon_m}\right) b_m + \left(\frac{L_{so}}{b_m}\right)\left(N_m - b_m\right) \tag{4.41}$$

which when combined with Equation (4.15) gives

$$\varepsilon_m = \ell n(e^{\varepsilon_s} + 1 - r_m) \tag{4.42}$$

Combination of this equation with Equation (4.20) then gives the unaxial representation

$$\frac{dr_m}{d\varepsilon_m} = e^{\varepsilon_s}(r_m b_m - 1) + (r_m - 1) \tag{4.43}$$

Substitution of Equation (4.40) or (4.43) into Equation (4.29) then gives

$$r_m(r_m b_m - 1)\left[\varepsilon_s - \ln r_m\right]^2 = R \tag{4.44}$$

for the multiaxial case, or

$$\left[e^{\varepsilon_s}(r_m b_m - 1) + (r_m - 1)\right]\left[\ln(e^{\varepsilon_s} + 1 - r_m)\right]^2 = R \tag{4.45}$$

for the uniaxial case, where

$$R = \frac{\left[\sigma_s\left(C\Psi \ln(\dot{\varepsilon}_o/\dot{\varepsilon}_s) - \frac{1}{1+\nu}\right) + \frac{\sigma_p}{1+\nu}\right](1-\phi_h)}{(G_h - G)\left[\frac{G + G_h^*}{G_h + G_h^*}\right]} \tag{4.46}$$

4.2.2 Calculations

Equations (4.44) to (4.46) were used to solve for the strain-dependent evolution of the controlling microstructure sizes, as follows. Strain rate versus strain data for the creep of pure aluminum at a shear stress of 3.0 MPa and 593°K were taken from Figure 2a of [37]. There were no strain data for $\varepsilon_s < 0.2$, so the initial value for computation was assumed to be 0.002, the point at which plastic deformation is generally considered to be fully developed. The strain history was thus ε_s = 0.002, 0.2, 0.3, 0.4, 0.5, 0.6, and the corresponding strain rate history was $\dot{\varepsilon}_s$ = 5 x 10^{-3}, 4.5 x 10^{-4}, 1 x 10^{-4}, 7 x 10^{-5}, 6 x 10^{-5}, 5.5 x 10^{-5} (sec^{-1}). Also, $\dot{\varepsilon}_o$ and Ψ were assumed to be 10^{-2}/sec and 1/3.1, respectively. The material constant C was again taken to be unity. The initial value of the shear modulus (G_o) was taken as

13.45 GPa, with Poisson's ratio $\nu = 0.347$. The remaining unknowns were then G_h, Φ_h, and σ_p as functions of ε_s. The stress polarization history was assumed to be $\sigma_p = 0.1, 0.1, 0.2, 0.3, 0.4, 0.5$. There were no data concerning the hardening fraction evolution with strain, although inspection of the micrographs in [37] resulted in the estimate $\Phi_h = 0.3$ at $\varepsilon_s = 0.6$. The assumed hardening fraction history was $\Phi_h = 0.025, 0.15, 0.2, 0.25, 0.275, 0.3$. G_h was assumed to be slightly larger than G_o, and is discussed in a later paragraph.

The above data were input to a small computer code that solved numerically for the scale factor $b_m = f(\varepsilon_s)$ at which the substructure controlled the macroscopic strain rate. This b_m was then used to calculate the evolution of the controlling substructure size L_m from Equation (4.13) with the reference length $L_{so} = 1$ cm:

$$L_m = e^{\varepsilon_s}/b_m \tag{4.47}$$

Results for both the uniaxial and multiaxial cases are shown in Figure 4.3, and agree reasonably well with available data, despite the large number of assumptions required to complete these preliminary calculations. At small strains, the controlling substructure size is close to the dislocation spacing for the estimated initial dislocation density of $10^6/cm^2$, a reasonable value for pure aluminum in the annealed state. The controlling substructure size (dislocation spacing) decreases rapidly as plastic deformation advances and the dislocation density increases drastically. There are no metallographic data for $\varepsilon_s < 0.2$, and the shaded area in Figure 4.3 indicates the anticipated range possible for randomly distributed peak dislocation densities between 10^8 and $10^{10}/cm^2$. At $\varepsilon_s = 0.05$ to 0.1, dislocation tangles would be expected to begin forming the walls of cells or subgrains. These walls would decrease in width as deformation advances, thus increasing the available path length for the motion of mobile dislocations within the cells or subgrains. This is indicated by the general upward trend in Figure 4.3, which begins to stabilize at larger strains, and results in a good prediction for the subgrain sizes found in [37].

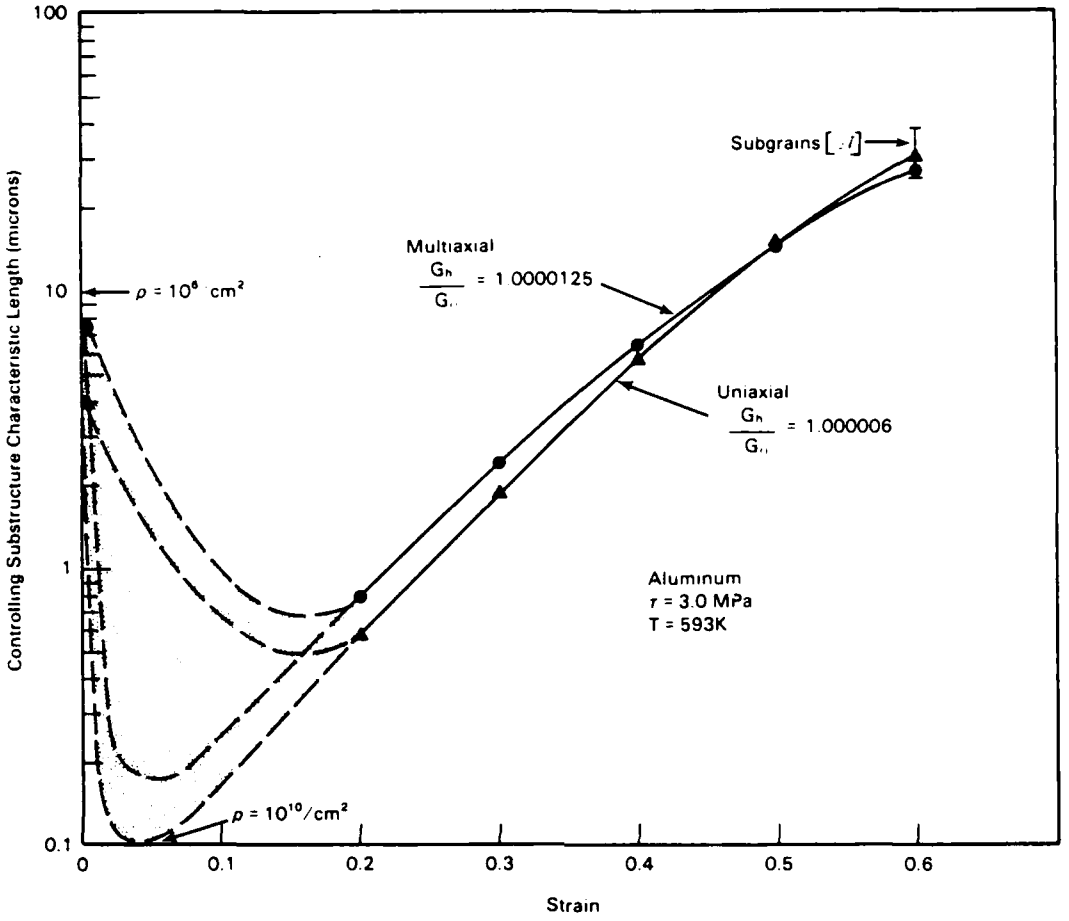

FIGURE 4.3. Predicted Evolution of Controlling Substructure for Creep of Aluminum at 3 MPa, 593°K

4.2.3 Relation to Physics and Metallurgy

The above results were obtained by assuming particular values for the ratio G_h/G_o, as shown in Figure 4.3. These values were found to be reasonable by the following arguments. G_o is the shear modulus of pure aluminum in the initial annealed state, while G_h is the modulus of the hardened phase (i.e., a cell wall) where dislocation densities are large (about $1.5 \times 10^9/cm^2$ [38,39]) and atomic bonds are elastically strained in an average sense. The force-displacement curve of atomic theory exhibits an increase in slope as the atoms are slightly separated [40]. This increase in interatomic force with small strains is manifested as an apparent increase in the effective modulus, which is defined as the ratio of stress (force per unit area) over strain. The force

increases in Figure 4.3 are 6×10^{-4} to 1.25×10^{-3} percent, and may not be easily measurable. However, analysis of the corresponding increase in strains is possible, as follows.

A "universal equation of state for metals" is available from [40], where the interatomic potential E is expressed as

$$E = E_o \, E^*(a^*) \tag{4.48}$$

where E_o is the equilibrium binding energy and

$$a^* = (r - r_e)/\ell \tag{4.49}$$

with r as the Wigner-Seitz radius, $r_e = 1.58 \times 10^{-8}$ cm is the equilibrium (zero strain) value of r for aluminum, and $\ell = 0.336 \times 10^{-8}$ cm is the normalization factor for aluminum. The normalized potential is

$$E^* = e^{-a^*} \, (1 + a^* + 0.05 \, a^{*3}) \tag{4.50}$$

The tangent modulus is proportional to $\Delta\sigma/\Delta\varepsilon$,

$$G = \frac{d\sigma}{d\varepsilon} = \frac{1}{A} \frac{dF}{d\varepsilon} \tag{4.51}$$

where the constant area A contains the Poisson factor and F is force. The strain is defined as

$$\varepsilon = a^* \ell / \ell_o \tag{4.52}$$

where $\ell_o = 4.04 \times 10^{-8}$ cm is the lattice constant. Thus,

$$G = \left(\frac{\ell_o}{A\ell}\right) \frac{dF}{da^*} \tag{4.53}$$

From $F = dE^*/da^*$, we have

$$\frac{G_h}{G_o} = \frac{(d^2E^*/da^{*2})_h}{(d^2E^*/da^{*2})_o} \tag{4.54}$$

so that E_o and the constants in Equation (4.53) cancel. Taking the required derivatives and assuming that $a_h^* > a_o^* = 0$, we have

$$\frac{G_h}{G_o} = e^{-a^*} (1 + 2.7a^* - a^{*2} - 0.65a^{*3} - 0.05a^{*5}) \tag{4.55}$$

Setting Equation (4.55) equal to 1.000006 or 1.0000125 yields $a^* = 3.5 \times 10^{-6}$ or 7.4×10^{-6} for the uniaxial and multiaxial cases in Figure 4.3, respectively. Equation (4.52) then gives the average elastic strains in the hardened phase; $\varepsilon_h = 2.9 \times 10^{-7}$ (uniaxial), $\varepsilon_h = 6.2 \times 10^{-7}$ (multiaxial). These values may be compared to the average strains associated with dislocations, as follows.

The volume fraction of dislocations in the hardened phase may be estimated as

$$V_f = \pi(\ell_o)^2 \rho = 7.7 \times 10^{-6} \tag{4.56}$$

Assuming that the material between the dislocations (whose spacing is $\rho^{-1/2} = 643\ \ell_o$) has zero elastic strain, and considering the dislocations as "fibers" so that the rule of mixtures applies, the strain associated with the dislocations is $\varepsilon_h/V_f = 0.037$ (uniaxial) or 0.081 (multiaxial). The shear strain associated with a screw dislocation is $b/2\pi\ell_o = 0.113$ ($b = 2.86 \times 10^{-8}$ cm is Burger's vector). The strain associated with a path around an edge dislocation is $b/8\ell_o = 0.088$. Therefore, the strains computed from the analysis of the

modulus changes (4 to 8%) compare reasonably well with those from a metallurgical analysis (9 to 11%). The factor of two discrepancy is easily accounted for by the uncertainties in the estimated dislocation density, and the approximation of a constant value for G_h over all scales. This lends support to the verification of the stress polarization equation.

4.3 DISCUSSION

The scale- and rate-dependent stress polarization (σ_p) equation was developed from Bodner's Equation using fractal scaling relations in a manner similar to the microstructural form developed in Section 3. The latter form (Equation 3.12) assumes that local behavior dominates with respect to scale, and requires microstructural models to predict the macroscopic strain rate. Conversely, the σ_p formulation (Equation 4.29) quantifies the nonlocal behavior as a function of scale. It requires no microstructural models, but needs certain state variable histories to predict the evolution of the internal stress field fluctuations as a function of the macroscopic stress and strain rate.

The preliminary verification results for aluminum (Section 4.2) showed that the σ_p equation could be used to predict the evolution of the microstructural features that control viscoplastic deformation, given the hardening and damage state variable histories. Although such data are sometimes available for larger strains, they frequently do not exist at smaller strains (where viscoplastic rate effects are most important) because of experimental difficulties. A method has been developed to alleviate this deficiency by eliminating ϕ_{hm} and ϕ_{dm} from the σ_p equation, leaving the stress polarization as a function of the chosen scale factor (b_m) and the macroscopic stress and strain rate. The resulting equation can then be solved to find the spectrum of scales over which nonlocal behavior dominates, thus providing guidance for metallographic analyses and possibly for metallurgical design.

Note that the σ_p equation contains the function $r_m = f(\phi_{hm}, \phi_{dm})$, which has two important features. First, concerning the verification results in Figure 4.3, it should be noted that [37] contains mention of a small fraction of the subgrains having cells with average diameters an order of magnitude

smaller than the subgrains. References [38, 39] also found substructure dominated by cells about 8 microns in diameter. It is suspected that more accurate and complete representations of r_m, and thus ε_m, would be more complicated mathematically, resulting in multiple solutions for b_m (branchings) that would predict both cells and subgrains. Second, r_m measures hardening and damage in terms of departures from unity. Expansion to multiaxial forms can provide a combined hardening/damage tensor that can be inserted into continuum formulations, thus completing the second objective in the first paragraph of the Summary.

5.0 CONCLUSIONS AND RECOMMENDATIONS

The following results were obtained during the course of this work:

- A new form of Bodner's viscoplastic constitutive equation was developed. This form (Equation 1.1 or 3.12) admits microstructural models in an organized and physically meaningful manner. It was verified by comparison to high temperature creep data for a steel alloy, and is expected to exhibit improved hardening behavior in computer simulations of structural performance. The origin of the empirically-determined stress exponent was also identified in terms of microstructural phenomena occurring at various characteristic length scales within a deforming material.
- A stress polarization equation for viscoplasticity was also developed from Bodner's Equation. This new formulation (Equation 1.2 or 4.29) describes the rate-dependent evolution of the internal stress field fluctuations in the material as a function of macroscopic stress and strain rate, two hardening and damage state variables, and the characteristic sizes of the rate-controlling microstructures. Preliminary verification was obtained for the creep of aluminum, and showed that the stress polarization equation is potentially useful for the prediction of microstructural evolution in terms of macroscopic stress-strain rate data. This equation also contains the basis for the development of a new material state tensor that simultaneously describes hardening and damage phenomena.

The following recommendations are also made:

- The verification results obtained herein are preliminary in nature, and further testing of the above equations is in order.
- Development of the stress polarization equation should be continued to (1) provide analytical tools capable of predicting microstructural evolution in terms of macroscopic response, thus giving guidance to metallographic analyses and reducing the costs of metallurgical design, and (2) complete the development of the combined hardening and damage state tensor.

6.0 ACKNOWLEDGMENTS

This research was sponsored by the Air Force Office of Scientific Research (AFSC) under contract F49620-85-C-0149. The United States Government is authorized to reproduce and distribute reprints for governmental purposes notwithstanding any copyright notation herein. The author wishes to thank Dr. Anthony Amos of the AFOSR Directorate of Aerospace Sciences for supporting this work, and Dr. C. H. Henager Jr. of Battelle Northwest for assistance in locating data for the example applications.

7.0 REFERENCES

1. S. R. Bodner and Y. Partom, "A Large Deformation Elastic-Viscoplastic Analysis of a Thick-Walled Spherical Shell," J. of Appl. Mech., Vol. 39, 1972, pp. 751-757.

2. S. R. Bodner and Y. Partom, "Constitutive Equations for Elastic-Viscoplastic Strain Hardening Materials," J. of Appl. Mech., Vol. 42, 1975, pp. 385-389.

3. S. R. Bodner, "A Hardness Law for Inelastic Deformation," Lett. in Appl. Eng. Sci., Vol. 16, 1978, pp. 221-230.

4. D. C. Stouffer and S. R. Bodner, "A Constitutive Model for the Deformation Induced Anisotropic Plastic Flow of Metals," Int. J. of Eng. Sci., Vol. 17, 1979, pp. 757-764.

5. D. C. Stouffer and S. R. Bodner, "A Relationship Between Theory and Experiment for a State Variable Constitutive Equation," in "Mechanical Testing for Deformation Model Development," R. W. Rhode and J. C. Swearingen, eds., ASTM STP 765, 1982, pp. 239-250.

6. M. H. Bohun and A. N. Palazotto, "Comparison of Two Viscoplastic Flow Laws as Applied to a Problem of Crack Growth," Engrg. Fract. Mech., Vol. 21, No. 3, 1985, pp. 503-519.

7. E. Krempl and V. V. Kallianpur, "Some Critical Uniaxial Experiments for Viscoplasticity at Room Temperature," J. of Mech. Phys. Solids, Vol. 32, No. 4, 1984, pp. 301-314.

8. B. B. Mandelbrot, "The Fractal Geometry of Nature," W. H. Freeman, Publ., 1982.

9. A. N. Norris, et al., "A Generalized Differential Effective Medium Theory," J. Mech. Phys. Solids, Vol. 33, No. 6, 1985, pp. 523-543.

10. A. N. Norris, "A Differential Scheme for the Effective Moduli of Composites," Mech. of Materials, Vol. 4, 1985, pp. 1-16.

11. J. C. Swearingen and J. H. Holbrook, "Internal Variable Models for Rate-Dependent Plasticity: Analysis of Theory and Experiment," Res Mechanica, Vol. 13, 1985, pp. 93-128.

12. Y. Chen, "Power-Formula Viscoplasticity, Its Modification and Some Applications," J. of Eng. Mat. and Tech., Vol. 106, 1984, pp. 383-387.

13. H. Ghoneim, et al., "Viscoplastic Modeling with Strain Rate History Dependency," J. of Appl. Mech., Vol. 50, 1983, pp. 465-468.

14. D. W. Nicholson and K. C. Kiddy, "A Large Deformation Plasticity Model with Rate Sensitivity and Thermal Softening," J. of Eng. Mat. and Tech., Vol. 106, 1984, pp. 388-392.

15. "Symposium on Constitutive Equations: Micro and Macro Aspects," ASME Winter Meeting, New Orleans, December 1984, J. of Eng. Mat. and Tech., Vol. 106, 1984, G. W. Weng, ed.

16. R. W. Rohde and J. C. Swearingen, Editors' Summary in "Mechanical Testing for Deformation Model Development," ASTM STP 765, 1982, p. 474.

17. J. R. Rice, "On the Structure of Stress-Strain Relations for Time-Dependent Plastic Deformation in Metals," J. of Appl. Mech., Vol. 37, 1970, pp. 728-737.

18. J. R. Rice, "Continuum Mechanics and Thermodynamics of Plasticity in Relation to Microscale Deformation Mechanisms," in "Constitutive Equations in Plasticity," A. S. Argon, ed., MIT Press, Cambridge, Massachusetts, 1975, pp. 23-75.

19. L. E. Malvern, "Introduction to the Mechanics of a Continuous Medium," Prentice-Hall, Inc., Inglewood Cliffs, New Jersey, 1969, pp. 368, 375, 379.

20. I. S. Kunin, "On Foundations of the Theory of Elastic Media with Microstructure," Int. J. Engrg. Sci., Vol. 22, No. 8-10, 1984, pp. 969-978.

21. E. Kroner, "Interrelations Between Various Branches of Continuum Mechanics," In: Mechanics of Generalized Continuua, IUTAM Symposium, 1968.

22. D. Rogula, "Non-Classical Material Continuua," Theo. and Appl. Mech., 1985, pp. 339-353.

23. S.-P. Hannula, et al., "Micromechanical Aspects of Deformation Theories Based on a State Variable Approach," Res Mechanica, Vol. 15, 1985, pp. 99-128.

24. R. Lagneborg, "A Modified Recovery-Creep Model and Its Evaluation," Met. Sci. Journal, Vol. 6, 1972, pp. 127-133.

25. R. Lagneborg, et al., "A Recovery-Creep Model Based Upon Dislocation Distributions," Trans. of Metals Soc., 1973, pp. 1-7.

26. A. Oden, et al., "Dislocation Distributions During Creep and Recovery of a 20%Cr-35%Ni Steel at 700°C," Trans. of Metals Soc., 1973, pp. 60-66.

27. R. Gasca-Neri and W. D. Nix, "A Model for the Mobile Dislocation Density," Acta Met., Vol. 22, 1974, pp. 257-264.

28. A. Orlova, "Mobile Dislocation Density in the Steady State Creep and in the Strain Transient Dip Test," Scripta Met., Vol. 13, 1979, pp. 763-766.

29. K. Keller, "Modeling Critical Behavior in Terms of Catastrophe Theory on Fractal Lattices," J. of Phys. A, Vol. 14, 1981, pp. 1719-1734.

30. Z. Hashin and S. Shtrikman, "A Variational Approach to the Theory of the Elastic Behavior of Polycrystals," J. Mech. Phys. Solids, Vol. 10, 1962, pp. 343-352.

31. Z. Hashin and S. Shtrikman, "On Some Variational Principles in Anisotropic and Nonhomogeneous Elasticity," J. Mech. Phys. Solids, Vol. 10, 1962, pp. 335-342.

32. J. R. Willis, "The Nonlocal Influence of Density Variations in a Composite," Int. J. Solids Structures, Vol. 21, No. 7, 1985, pp. 805-817.

33. W. Kreher and W. Pompe, "Field Fluctuations in a Heterogeneous Elastic Material - An Information Theory Approach," J. Mech. Phys. Solids, Vol. 33, No. 5, 1985, pp. 419-445.

34. D.G.B. Edelen, "Forces on Dislocations and Inhomogeneities in the Gauge Theory of Defects," Int. J. Solids Structures, Vol. 21, No. 7, 1985, pp. 699-710.

35. E. Kroner, "Incompatibility, Defects and Stress Functions in the Mechanics of Generalized Continuua," Int. J. Solids Structures, Vol. 21, No. 7, 1985, pp. 747-756.

36. D. J. Bergman and Y. Kantor, "Critical Properties of an Elastic Fractal," Phys. Rev. Lett., Vol. 53, No. 6, 1984, pp. 511-514.

37. T. J. Ginter, et al., "Effect of Creep Substructure on the Stress Exponent of Al Following Stress Reductions," Phil. Mag. A, Vol. 50, No. 1, 1984, pp. 9-24.

38. A. Orlova, et al., "Internal Stress and Dislocation Structure of Aluminum in High Temperature Creep," Phil. Mag. A, Vol. 26, 1972, pp. 1263-1274.

39. A. Orlova and J. Cadek, "Some Substructural Aspects of High Temperature Creep in Metals," Phil. Mag. Vol. 28, 1973, pp. 891-899.

40. J. H. Rose, et al., "Universal Features of the Equation of State for Metals," Phys. Rev. B, Vol. 29, No. 6, 1984, pp. 2963-2969.

41. J. F. Bell, "Contemporary Perspectives in Finite Strain Plasticity," Int. J. Plasticity, Vol. 1, No. 1, 1985, pp. 3-27.

APPENDIX

THE CONSERVATION OF MASS APPROACH

APPENDIX

THE CONSERVATION OF MASS APPROACH

This approach was an attempt to solve for the dimensionalities in Equation (4.1), as follows. The conservation of mass equation requires that the material derivative of the mass is zero. Expressing the mass m as the density times the fractal volume, this is

$$\frac{dm}{dt} = \frac{\partial}{\partial t}\left(\rho L^D\right) + v_i \frac{\partial}{\partial x_i}\left(\rho L^D\right) = 0 \qquad (A.1)$$

where the small d represents the material derivative and the summation convention applies in the last term.

Performing the derivatives, this equation becomes

$$L^D\left(\frac{\partial \rho}{\partial t} + v_i \frac{\partial \rho}{\partial x_i}\right) + \rho\left(\frac{\partial L^D}{\partial t} + v_i \frac{\partial L^D}{\partial x_i}\right) = 0 \qquad (A.2)$$

The usual conservation of mass equation gives

$$\frac{\partial \rho}{\partial t} + v_i \frac{\partial \rho}{\partial x_i} = -\rho \frac{\partial v_i}{\partial x_i} \qquad (A.3)$$

which can be substituted into Equation (A.2) to give a differential equation for the fractal volume (L^D):

$$\frac{\partial L^D}{\partial t} + v_i \frac{\partial L^D}{\partial x_i} = L^D \frac{\partial v_i}{\partial x_i} \qquad (A.4)$$

where the L above is a suitable average of the characteristic lengths of the three principal directions

$$L_x = L_o\, e^{\varepsilon_x} \qquad (A.5)$$
$$L_y = L_z = L_o\, e^{-\nu\varepsilon_x}$$

where L_o is the initial length, and ν is Poisson's ratio. Equations (A.4) and (A.5) are assumed to be valid for any scale within the material. The x_i and v_i in Equation (A.4) are defined by Equations (A.5) and their derivatives.

The choice of the average length L determines the final form of the differential equation for D. A number of attempts were made to find a suitable representation of L, with inconsistent results. Examples are choices based on the strain invariants (i.e., I_E) and the strain deviator invariants (i.e., $II_{E'}$):

$$L = L_o\, (I_E - II_E + III_E + 1)^{1/3} \qquad (A.6)$$

$$L = L_o\, (II_{E'} + III_{E'} + 1)^{1/3} \qquad (A.7)$$

The final differential equation for D on any scale corresponding to, i.e., Equation (A.7) was

$$\left[3r\, \ell n\left(L_o\, A^{1/3}\right)\right] \frac{\partial D}{\partial r} + \frac{4BD}{3} = 1-2\nu \qquad (A.8)$$

with

$$r = \exp\,(\varepsilon_x) \qquad (A.9)$$

and

$$A = \alpha\varepsilon_x^{\,2} + \beta\varepsilon_x^{\,3} + 1$$

$$B = \left(2\alpha\varepsilon_x + 3\beta\varepsilon_x^{\,2}\right)/A \qquad \text{(A.10)}$$

$$\alpha = -1/3\ (1+2\nu+\nu^2)$$

$$\beta = 2/9\ (1+3\nu-21\nu^2+\nu^3)$$

where Poisson's ratio ν depends on the dimensionality D [36]

$$\nu = \frac{6 - D}{12 + D} \qquad \text{(A.11)}$$

The differential equation corresponding to Equation (A.6) was similar, but with different versions of Equations (A.10).

Given a characteristic length L_o corresponding to a chosen scale, differential equations such as Equation (A.8) were solved numerically and the results represented in the form of plots of macroscopic strain rate versus strain. This was done by approximating the constitutive equation by the form

$$-C\ \ell n\left(\dot{\varepsilon}_s/\dot{\varepsilon}_o\right) \approx \left[\left(\frac{1}{a_o} + \frac{f(D_a)}{b_o}\right)\Big/ a_o^{\,D_a}\right]\left[\frac{E_o}{\Psi\ \sigma_s b_o\ \rho_m}\right] \qquad \text{(A.12)}$$

where a_o is a lattice constant, b_o is a Burger's vector, Ψ is the Schmid factor, E_o is atomic binding energy, and ρ_m is the mobile dislocation density. The term $f(D_a)$ represents damage on the atomic scale, and is developed from a rearrangement of Equation (A.8) so that

$$f(D_a) = \frac{\partial\ \ell n\left(L_a^{\,D_a}\right)}{\partial t} \qquad \text{(A.13)}$$

Note that $L_s {}^{D}s$ is omitted from Equation (A.12) because it is assumed relatively constant, consistent with the observation of volume conservation on the macroscopic scale [41]. Setting the last term in Equation (A.12) equal to a constant, the basic strain rate versus strain behavior can be observed as shown in Figure A.1. The ordinate in this figure is the macroscopic strain rate normalized to the value at the assumed starting strain (10^{-5}). The abscissa is the strain on the scales noted in the figure.

The two solutions in Figure A.1 show quite different results depending on the representation of L chosen. Another representation with $I_E = 0$ in Equation (A.6) [41] gave results similar to the "strain invariant" curves shown in the figure. Note that both solutions show macroscopic effects at much smaller strains than for the microscopic scale. This may be somewhat consistent with the following observation. Although a small permanent deformation of the macroscopic sample may be measurable, a random microscopic sample will frequently show no obvious evidence of such deformation, at least for the relatively small macroscopic strains over which viscoplasticity is important. However, the monotonic behavior of either solution in Figure A.1 was taken as an indication that hardening and damage were actually not simultaneously represented, as originally intended. This is also obvious from Equation (A.12), where the damage term may be represented by the first bracket and the hardening behavior by ρ_m in the second bracket. In essence, the continuum and metallurgical contributions had remained separated. The consequent failure of the above conservation of mass approach thus indicated that another direction should be taken, and the stress polarization approach was subsequently adopted.

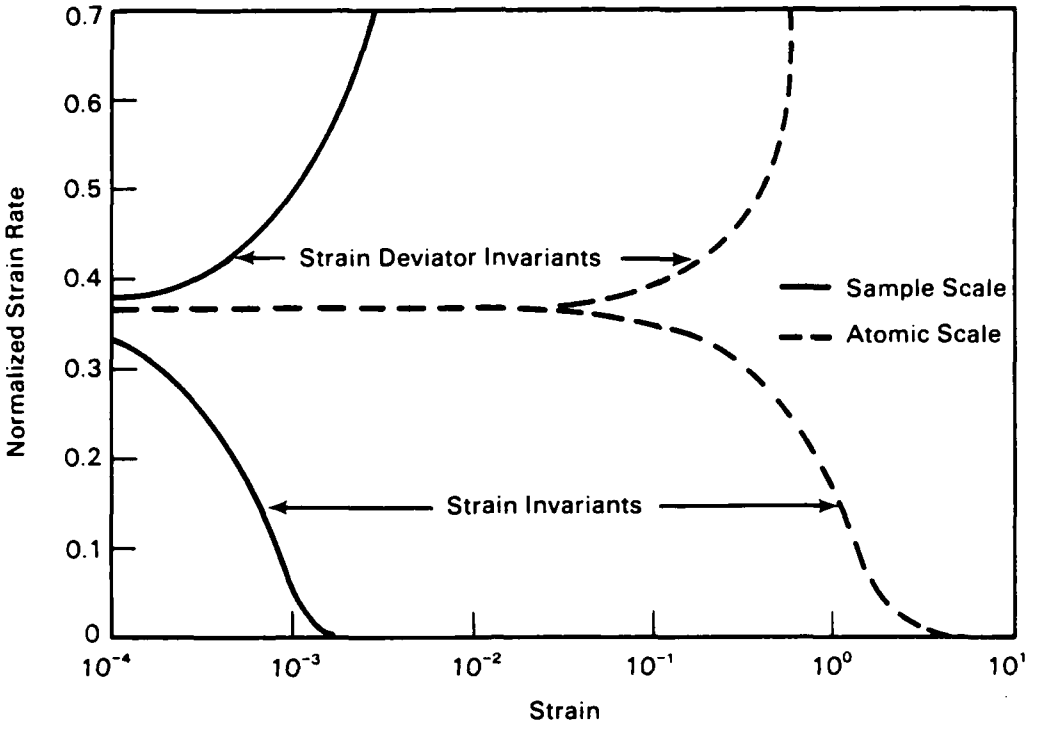

FIGURE A.1. Results of the Conservation of Mass Approach

END

1-87

DTIC